Available online at www.sciencedirect.com
SCIENCE DIRECT®
Journal of Solid State Chemistry 177 (2004) 817–823
JOURNAL OF SOLID STATE CHEMISTRY
http://elsevier.com/locate/jssc

Crystal structure, oxidation state and magnetism of $La_{1.2}Sr_{2.4}RuO_7$: a new member of the $[A_2O][A_nB_{n-1}O_{3n}]$ series of hexagonal perovskites

Stefan G. Ebbinghaus*

Lehrstuhl für Festkörperchemie, Institut für Physik, Universität Augsburg, Universitätsstraße 1, D-86159 Augsburg, Germany

Received 30 June 2003; received in revised form 6 September 2003; accepted 12 September 2003

Abstract

Single crystals of the new compound $La_{1.2}Sr_{2.4}RuO_7$, an oxide related to the hexagonal perovskites, were grown from a $BaCl_2$ flux. The structure was solved by single crystal X-ray diffraction. $La_{1.2}Sr_{2.4}RuO_7$ crystallizes in the space group $R\bar{3}m$ with $a = 5.760(1)$ Å and $c = 18.273(3)$ Å. It is one of the rare examples of oxides with isolated RuO_6-octahedra. The structure consists of alternating layers of RuO_6-octahedra and trigonal (La,Sr)O_6-prisms. These prisms are capped by one additional oxygen ion, which occupies a distorted position within the (La,Sr)O_6-layers. $La_{1.2}Sr_{2.4}RuO_7$ is the second member of the general $[A_2O][A_nB_{n-1}O_{3n}]$ family of hexagonal perovskites with $n = 2$ and the first ruthenate possessing this structure. XANES investigations, bond valence sum calculations and magnetic measurements show that ruthenium takes the oxidation state $+5$. Although the ruthenium ions have quite long distances, a medium strong antiferromagnetic interaction between these paramagnetic centers was observed.

Keywords: Hexagonal perovskites; Ruthenates; Single crystal structure; XANES; Oxidation states; Magnetic properties

1. Introduction

Perovskite oxides (general composition ABO_3) are usually described as a 3D-network of corner-sharing BO_6-octahedra with the A-type cations occupying the cuboctahedral sites formed by this arrangement. In an alternative description, the perovskite structure can be considered as a cubic close packing (stacking sequence *abcabc*…) of AO_6-units with the B-cations occupying the octahedral vacancies. A changing of the stacking sequence to a hexagonal close packing (*ababab*…) leads to the family of so-called hexagonal perovskites, which have the same composition (ABO_3) but in which the BO_6-octahedra share common faces. The most basic structure of this family—the so-called 2H polytype—consists of infinite chains of face-sharing BO_6-octahedra, isolated by chains of AO_{12}-units. If parts of the AO_3-layers are replaced by $AA'O_2$-layers, triangular $A'O_6$-prisms are formed. This leads to a family of compounds with the general formula $A_{3m+3n}A'_nB_{3m+n}O_{9m+6n}$. In these oxides, stacks of face-sharing BO_6-octahedra are connected by $A'O_6$-prisms [1]. Ref. [2] gives an overview of known members of this type of hexagonal perovskites and their structural relationships.

In the course of a systematic study on lanthanum and strontium containing ruthenates, a new compound with the (slightly simplified) composition $La_{1.2}Sr_{2.4}RuO_7$ was found (Fig. 1). It turned out that its structure is very similar to the $n = 1, m = 0$ end member of the above mentioned series. Like this polytype, which is often denoted as the Sr_4PtO_6 structure, it is built of isolated BO_6-octahedra whose trigonal faces form the basis of triangular prisms. The differences between the two structures result from a different stacking mode along the *c*-axis, leading to an additional layer component in $La_{1.2}Sr_{2.4}RuO_7$. This intermediate layer has the composition $(La,Sr)_2O$. The title compound can therefore be considered the $n = 2$ member of a whole family of hexagonal perovskites with the general formula $[A_2O][A_nB_{n-1}O_{3n}]$. In this formula, $n-1$ reflects the number of face-sharing BO_6-octahedra [3]. The $n = 3$ member of this series is represented by $Ba_5Ru_2O_{10}$ [4], while to the best of our knowledge the only $n = 2$ compound known so far is $La_2Ca_2MnO_7$ [5]. For the latter two samples it was also found possible to replace the A_2O-layers by $A_2(O_2)$-layers, i.e. these oxides contain peroxide units (O_2^{2-}) [6,7]. In an even more

*Fax: +49-821-598-3002.
E-mail address: stefan.ebbinghaus@physik.uni-augsburg.de.

0022-4596/$ - see front matter © 2003 Elsevier Inc. All rights reserved.
doi:10.1016/j.jssc.2003.09.035

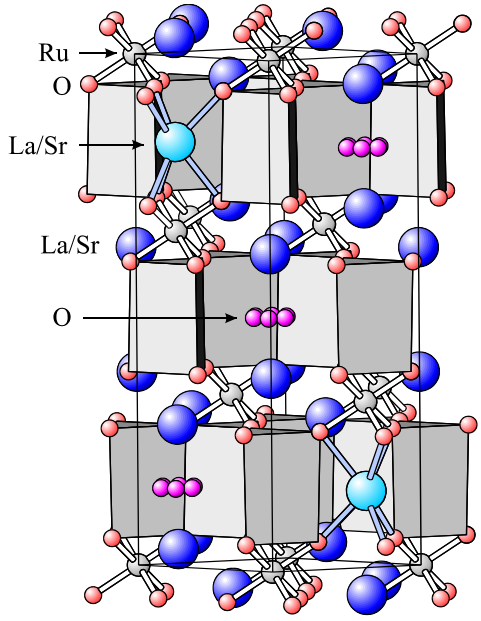

Fig. 1. Structure of $La_{1.2}Sr_{2.4}RuO_7$. Two of the (La,Sr)O_6-prisms are shown without faces to emphasize the coordination geometry.

generalized description the composition can therefore be summarized as $[A_2O_{2-\delta}][A_nB_{n-1}O_{3n}]$, where $\delta = 1$ corresponds to the oxide and $\delta = 0$ to the peroxide, respectively [7]. It is noteworthy that the substitution of O^{2-} for O_2^{2-} does not change the oxidation state of the transition metal involved.

2. Experimental

Single crystals of the title compound were unintentionally grown in an attempt to crystallize $La_{0.84}Sr_{1.16}Cu_{0.7}Ru_{0.3}O_{4-\delta}$ using $BaCl_2$ as a mineralizer. The starting material was prepared by solid state reaction as described in Ref. [8]. 0.5 g of this Ruddlesden-Popper type oxide was thoroughly ground with 0.4 g $BaCl_2$ and heated in air in a platinum crucible at 1250°C for 36 h. The temperature was then reduced to 900°C at a rate of 10°C/h. Finally, the furnace was switched off and allowed to cool down. The obtained crystals were washed with water several times to remove remaining flux.

For single crystal structure analysis a Syntex $P2_1$ diffractometer operating with Mo$K\alpha$ radiation was used. Cell constants were determined from a least-squares refinement of 25 reflections collected in the range $19° < 2\theta < 30°$.

The intensities of 5553 reflections were measured in the angular range $4.5° < 2\theta < 85°$. Three check reflections were remeasured after each 100 reflections. The crystal shape was approximated by 8 faces and the observed intensities were absorption corrected using the analytical approach by de Meulenaer and Tompa [9]. For structure solution and refinement the programs ShelXS97 and ShelXL97 [10,11] were used. Experimental details of the structure analysis can be found in Table 1.

Table 1
Crystal data and structure refinement for $La_{1.2}Sr_{2.4}RuO_7$

Diffractometer	Syntex $P2_1$
Temperature	293 K
Wavelength	0.71073 Å
Crystal system, space group	Trigonal, $R\bar{3}m$ (#166)
Unit cell dimensions	$a = 5.7600(9)$ Å
	$c = 18.273(3)$ Å
Volume	525.03(14) Å^3
Z, Calculated density	3, 5.993 g cm^{-3}
Absorption coefficient	31.12 mm^{-1}
$F(000)$	805
Crystal size	$0.25 \times 0.16 \times 0.08$ mm^3
θ range for data collection	3.34–42.61°
Index ranges	$-10 \leqslant h \leqslant 10$
	$-10 \leqslant k \leqslant 10$
	$-34 \leqslant l \leqslant 34$
Reflections collected/unique	5553/514 [R(int) = 0.0233]
Completeness to $2\theta = 42.45$	100.0 %
Refinement method	Full-matrix least-squares on F^2
Data/restraints/parameters	514/3/33
Goodness-of-fit on F^2	1.209
Final R indices [$I > 2\sigma(I)$]	$R_1 = 0.0288$, w$R_2 = 0.0672$[a]
R indices (all data)	$R_1 = 0.0295$, w$R_2 = 0.0677$[a]
Extinction coefficient	0.0059(4)
Largest diffraction Peak and hole	2.312 and −2.001 e A^{-3}

[a] $w = 1/[\sigma^2(F_o^2) + (0.0237P)^2 + 9.7865P]$ where $P = (F_o^2 + 2F_c^2)/3$.

XANES investigations at the Ru–L_{III} edge were carried out at the beamline E4 of the Hamburger Synchrotronstrahlungslabor (HASYLAB) at the Deutsches Elektronensynchrotron (DESY).

A powder of some well-ground crystals was stuck to adhesive tape, which was folded three times to yield the desired increase of absorption of $\Delta\mu \approx 2$ at the Ru–L_{III} threshold. The measurements were performed in transmission mode with a step width of 0.1 eV and a counting time of 2 s per data point. The energy was calibrated against the spectrum of Ru metal (2.8380 keV), which was remeasured before and after the sample and after each new beam injection. Data reduction and fit of the Ru–L_{III} edge XANES region were carried out as described in detail in Ref. [12].

Magnetic measurements in the temperature range $2\,K < T < 300\,K$ were done on a Quantum Design MPMS-SQUID at 0.01 and 1 T, respectively. The obtained values were corrected for the diamagnetic moment of the empty sample holder.

For element analysis a Camebax-Microbeam electron microprobe analyzer was used. $SrTiO_3$, $BaSO_4$, monazite, copper-, ruthenium- and platinum-metal were taken as internal standards for Sr, Ba, La, Cu, Ru and Pt, respectively.

3. Results and discussion

3.1. Crystal structure

The obtained crystals had typical dimensions of $0.2 \times 0.2 \times 0.05\,mm^3$ and possessed a rhombohedral shape. EMA measurements on seven crystals led to the following average composition: $La_{1.20(4)}Sr_{2.42(5)}Ru_{0.96(5)}Pt_{0.04(5)}O_{6+\delta}$. It is worth noting that the results for the different crystals were almost identical within the standard deviations given in brackets and that neither copper nor chlorine was found. Although the crystals were grown from a $BaCl_2$ flux, the Ba concentration was found to be very small (<2% of the A-type cations) and was therefore neglected. The small Pt content is obviously due to the crucible used for the crystal growth.

Since the experimentally determined composition is rather complex, a simplified stoichiometry is used in the following, i.e. the compound is referred to as $La_{1.2}Sr_{2.4}RuO_7$.

The reflection conditions observed in the single crystal X-ray diffraction led to the possible space groups *R*32, *R*3*m*, and $R\bar{3}m$. Structural refinements were carried out in $R\bar{3}m$. Attempts to refine the structure in the other two space groups did not improve the results. A 4% substitution of ruthenium by platinum was included in the refinement. An unrestrained fit yielded a too small lanthanum content, therefore the sum of La and Sr ions was fixed to the values found in the EMA analysis, allowing a tolerance of 0.5%. This procedure caused only a minimal increase of the residual indices.

To avoid a nonsensical site occupation factor larger than 1 for the La1/Sr1 position (see Table 2), the sum of the fractional La and Sr occupation factors was fixed to unity. The La2/Sr2 position (which corresponds to A-type cations within a trigonal prismatic oxygen coordination) was first refined with Sr and La occupying the $(0,0,z)$ position only. This gave rise to a very large and strongly oblate displacement parameter and a considerable remaining electron density at approximately (0.1, 0.05, 0.175). Positioning the ions at this position resulted in non-positive displacement parameters. Therefore, we used a split model with parts of the A-type cations at the position $(0,0,z)$ and parts at $(2x,x,z)$ with $x \approx 0.05$, $z \approx 0.175$. This led to reasonable displacement parameters for both sites and a considerable reduction of the *R*-values. This model is supported by the fact that a similar distortion of the A-cations within the trigonal prisms was already found for $Ba_5Ru_2O_9(O_2)$ [6]. Attempts to additionally place some of the La-ions on the *18h* position led to unstable refinement runs. We therefore conclude that the off-center position in the trigonal prisms is only occupied by Sr-ions. It is worth noting that the sum of the La2, Sr2 and Sr2a site occupation factors only leads to a 80% occupation of the position within the trigonal prisms, while the remaining 20% sites apparently stay vacant.

Six of the triangular prisms form a hexagonal cavity (Fig. 2). Difference Fourier transforms revealed the presence of donut-shaped remaining electron density in the center of these cavities. This electron density could be described by a distorted oxygen ion located at $(x,0,\frac{1}{2})$ as shown in Fig. 2. A refinement of the occupation factor yielded a value of 0.16, which is very close to $\frac{1}{6}$. The O2 site is thus occupied by one oxygen ion per unit cell, leading to a total oxygen content of 7.

Positioning the O2 ion at $(x,-x,\frac{1}{2})$ instead of $(x,0,\frac{1}{2})$ resulted in a strongly elongated displacement parameter

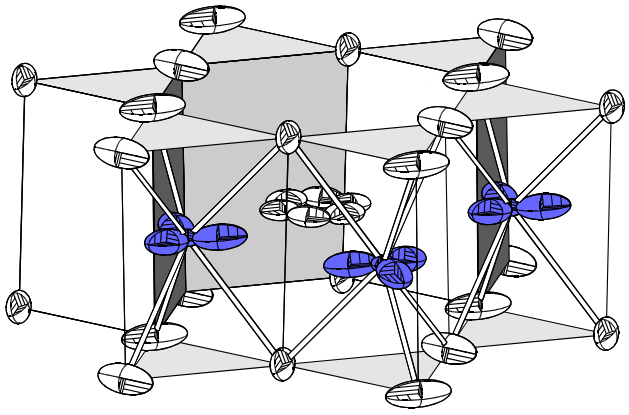

Fig. 2. Detailed view of the crystal structure showing the trigonal (Sr2,La2)O_6-units and the distorted O2-ions. Thermal ellipsoids are shown at the 50% confidence level.

Table 2
Atomic coordinates and equivalent isotropic displacement parameters for $La_{1.2}Sr_{2.4}RuO_7$

Atom	Site	SOF	*x*	*y*	*z*	U_{eq} (Å^2)
Ru/Pt	3*a*	0.96/0.04	0.	0.	0.	0.0079(1)
O1	18*h*	1.0	0.3200(8)	0.1600(4)	0.0616(2)	0.061(2)
Sr1/La1	6*c*	0.620(8)/0.380(8)	0.	0.	0.62180(2)	0.0141(1)
Sr2/La2	6*c*	0.33(3)/0.211(7)	0.	0.	0.17472(8)	0.0148(7)
Sr2a	18*h*	0.085(11)	0.110(11)	0.055(5)	0.1768(5)	0.048(8)
O2	18*g*	0.160(10)	0.110(5)	0.	0.5	0.038(10)

U_{eq} is defined as one-third of the trace of the orthogonalized U_{ij} tensor.

Table 3
Anisotropic displacement parameters (Å^2) for $La_{1.2}Sr_{2.4}RuO_7$

Atom	U_{11}	U_{22}	U_{33}	U_{23}	U_{13}	U_{12}
Ru/Pt	0.0058(1)	0.0058(1)	0.0122(2)	0	0	0.0029(1)
O1	0.0144(15)	0.1110(50)	0.0247(16)	−0.0023(6)	−0.0046(13)	0.0072(7)
Sr1/La1	0.0170(2)	0.0170(2)	0.0084(2)	0	0	0.0085(1)
Sr2/La2	0.0181(9)	0.0181(9)	0.0082(5)	0	0	0.0090(4)
Sr2a	0.090(20)	0.047(6)	0.020(3)	0.004(2)	0.008(5)	0.045(12)
O2	0.049(13)	0.060(20)	0.011(5)	0.003(7)	0.001(3)	0.028(11)

The anisotropic displacement factor exponent takes the form: $-2\pi^2[h^2a^{*2}U_{11} + \cdots + 2hka^*b^*U_{12}]$.

for this atom. We therefore conclude that the *18g* position is better suited to describe the distorted oxygen.

The displacement ellipsoid for the O1 ion was found to be rather elongated. Attempts to refine this site with a split oxygen position did not lead to stable results. Obviously, the observed oxygen displacement parameter actually reflects a distortion, i.e. a rotation of the RuO_6-octahedra around the crystallographic *c*-axis.

To verify that there was no overlooked ordering within the structure we sought for additional diffraction peaks. Therefore, we did single crystal X-ray diffraction measurements on an imaging plate diffractometer (STOE IPDS II, Ag$K\alpha$ radiation). To enhance the resolution of the diffractometer, the imaging plate was adjusted at a rather long distance of 150 mm. Furthermore, electron diffraction experiments were performed on a Philips CM10 TEM operating at 120 keV. The diffraction patterns along various zone axes were recorded. No satellite reflections were observed in either of these two methods. This result confirms that $La_{1.2}Sr_{2.4}RuO_7$ does not possess an incommensurate structure or a superstructure. Instead it seems that the split Sr2a and O2 positions are indeed statistically equally occupied.

The final refinement run included anisotropic displacement parameters for all atoms and converged smoothly to the *R*-values listed in Table 1. Atomic coordinates and equivalent isotropic displacement parameters are listed in Table 2, while Tables 3 and 4 give the anisotropic displacement parameters and selected bond lengths, respectively.

Due to the local $\bar{3}m$ symmetry of the Ru ions all six Ru–O1 distances must be equal but a trigonal distortion of the octahedra is possible. However, the observed O1–Ru–O1 angles of 90.1(2)° indicate that the RuO_6-units are almost ideal octahedra. This observation is in agreement with the proposed Ru^{+5} oxidation state (see discussion below). The resulting $^4A_{2g}$ electronic ground state has no orbital degeneracy and therefore no Jahn–Teller distortion is expected.

The Ru−O1 bond length can be compared with its value calculated from the bond valence sum theory. Following this general approach, the total valence of a cation (V_i) is given by the sum of the valences of its bonds $V_i = \Sigma_j(v_{ij})$. The commonly used empirical expression for these bond valences is $v_{ij} = \exp[(R_{ij} - d_{ij})/0.37]$ [13], where d_{ij} is the bond length and R_{ij} is the empirical bond valence parameter. Using the value of 1.888 for $R_{RU^{+5}-O}$ given in Ref. [14], a distance of 1.953 Å is expected, which is in excellent agreement with the result from the crystal structure analysis (1.953(4) Å). The experimentally found bond length is therefore a strong confirmation of the magnetic and XANES results discussed below.

Table 4
Selected bond lengths (Å)

6× Ru–O1	1.953(4)
3× Sr1/La1−O1	2.603(5)
6× Sr1/La1−O1	2.897(1)
1× Sr1/La1−O2	2.314(8)
3× Sr2/La2−O1	2.477(4)
3× Sr2/La2−O1	2.611(5)
1× Sr2/La2−O2[a]	2.800(5)

[a] Only the shortest distance to the 6 distorted oxygen positions is given.

An unusual connection between BO_6-octahedra and AO_6-prisms is found in $La_{1.2}Sr_{2.4}RuO_7$: One triangular plane of the prisms shares a common face with one RuO_6-octahedron while the opposite plane is corner-sharing with three additional octahedra. This structural detail is shown in Fig. 3.

Compared to the bond lengths Sr1/La1−O1 (2.897 and 2.603 Å, respectively), the distance Sr1/La1−O2 is quite short (2.314(8) Å). Since there are 6 identical distances but the site occupation factor is $\frac{1}{6}$, only one bond actually exists. The same consideration can be applied to the La2/Sr2 ion, again leading to an average value of only one La2/Sr2−O2 bond (see Table 4). Fig. 4 shows the oxygen coordination of the La- and Sr-ions. For sake of clarity, bonds are not drawn to all of the O2 ions, and for the Sr2/La2/Sr2a-unit only the Sr2a ions and their nearest oxygen neighbors are shown.

In principal, the O2 atoms may also belong to a peroxide unit (O_2^{2-}) like in $Ba_5Ru_2O_9(O_2)$ [6]. This interpretation is disfavored by the fact that the O–O

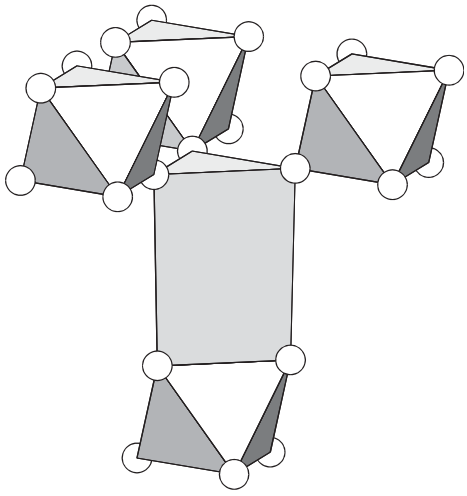

Fig. 3. Connection between triangular prisms and octahedra in $La_{1.2}Sr_{2.4}RuO_7$.

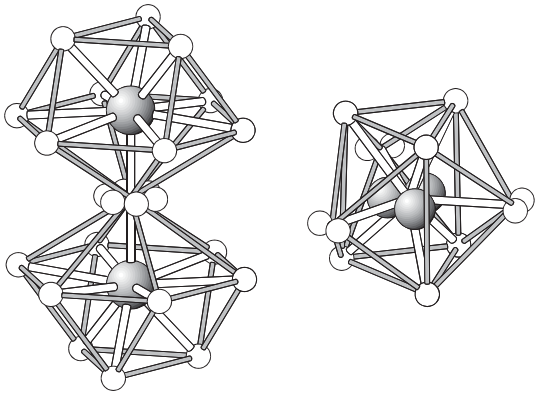

Fig. 4. Oxygen environments of the Sr/La ions. The left side shows the 10-fold oxygen coordination of the Sr1/La1 site, while the capped trigonal oxygen prisms around the Sr2/La2 ions are shown on the right side.

distance within the assumed peroxide unit would be 1.26(6) Å, a value much smaller than expected. For example, the O–O distances in the related peroxide compounds $Ba_5Nb_2O_9(O_2)$ and $Ba_5Ru_2O_9(O_2)$ are 1.619 Å [3] and 1.402 Å [6], respectively.

A representation of the complete crystal structure of $La_{1.2}Sr_{2.4}RuO_7$ is given in Fig. 5. The right side of the figure shows the structure of $Ba_5Ru_2O_{10}$. This compound can be considered to be the $n = 3$ homologue of the title compound. The similarities between the two structures—especially the common A_2O-layers—can clearly be seen.

To the best of our knowledge $La_{1.2}Sr_{2.4}RuO_7$ is the first ruthenium based $n = 2$ member of the $[A_2O][A_nB_{n-1}O_{3n}]$ family of hexagonal perovskites. Furthermore, $La_2Ca_2MnO_7$ is to date the only other oxide with an analogue structure. Unlike this compound, $La_{1.2}Sr_{2.4}RuO_7$ is a cation deficient perovskite with a considerable fraction of the trigonal prismatic sites remaining vacant. While $La_2Ca_2MnO_7$ has so far only been prepared as polycrystalline powder we here describe for the first time the single crystal structure refinement of a $[A_2O][A_2BO_6]$ perovskite.

3.2. Magnetism

The inverse magnetic susceptibilities measured with external fields of 1 and 0.01 T, respectively are shown in Fig. 6. No significant differences between field cooled and zero-field cooled values were observed. The magnetic behavior can be well fitted with a Curie–Weiß law in the range $50\,K < T < 300\,K$. A very small temperature-independent paramagnetic moment was added in the fit. Numerical results are shown in the figure. The paramagnetic moment of $3.32\mu_B$ per Ru ion (at $B = 1$ T) is somewhat smaller than expected but still in reasonable agreement with the value of $3.87\mu_B$ calculated for Ru^{+5}. The interpretation of the magnetic data is, on the other hand, not straightforward because of the small Pt content. For this metal the oxidation state is not known and thus its contribution to the magnetic moment cannot easily be estimated.

The negative Weiss constant of $\theta = -68$ K and a slight kink in the susceptibility data at $T = 15$ K reveal a considerable antiferromagnetic correlation between the ruthenium ions. This is rather surprising because the distances between one paramagnetic center and its nearest and next-nearest neighbors are 5.76 and 6.94 Å, respectively. Apparently, this separation is not sufficient to completely suppress the interaction of the magnetic moments. Similar values of θ (-58 and -85 K) were found in $La_7Ru_3O_{18}$ and $La_{4.87}Ru_2O_{12}$, two layered compounds in which the Ru ions have comparable distances ranging from 5.52 to 5.96 Å [15]. The Ru valence in $La_7Ru_3O_{18}$ and $La_{4.87}Ru_2O_{12}$ is $+5$ and $+4.7$, respectively. These values are identical or at least close to the one observed for $La_{1.2}Sr_{2.4}RuO_7$. Actually, bond valence calculations indicate that in $La_{4.87}Ru_2O_{12}$ half of the ruthenium ions have the oxidation state $+5$ while the other half have a mixed oxidation state of $+4.4$. Although these examples are too few to draw a general conclusion, the observed medium-strength antiferromagnetic interaction seems to be characteristic for isolated $Ru^{+5}O_6$-octahedra.

3.3. XANES

X-ray absorption near edge structure spectroscopy (XANES) is a highly useful tool to determine the oxidation state of transition metal ions because for a specific element the energies of the absorption edges increase with increasing charge. This so-called valence shift results from the fact that the positive electric charge of the nucleus is partially shielded by the d-electrons. An oxidation of the metal reduces the number of valence

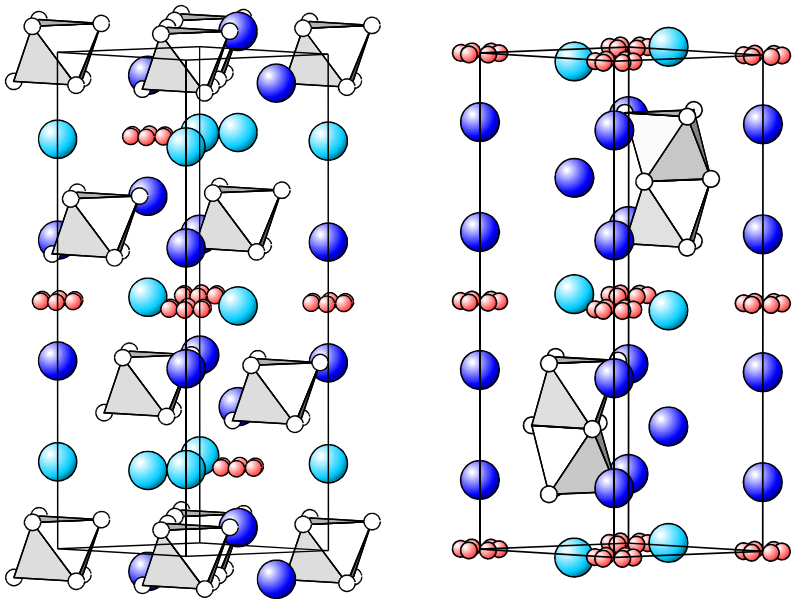

Fig. 5. Comparison between the crystal structure of $La_{1.2}Sr_{2.4}RuO_7$ (left) and $Ba_5Ru_2O_{10}$ (right).

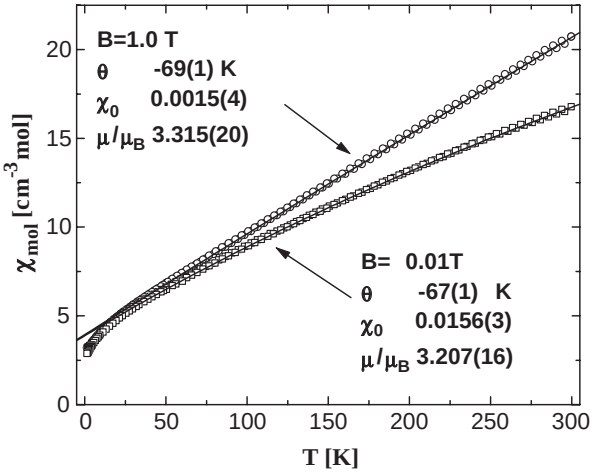

Fig. 6. Temperature dependence of the reciprocal magnetic susceptibility of $La_{1.2}Sr_{2.4}RuO_7$. Solid lines represent the fit of the data.

electrons. Consequently, the effective core charge increases and the inner electrons become more tightly bound, leading to a shift of the absorption edge towards higher energies. Examples for this effect in ruthenium containing perovskites can be found in Refs. [12,16]. L_{III} and L_{II} edges of transition metals are especially suited for the observation of the valence shift because they show very intense "white lines", which result from inner-atomic transitions of the $2p$ core electrons to unoccupied bound states with predominantly d-character ($l = 2$). A detailed examination of the Ru$-L_{III,II}$ absorption edge reveals the presence of two peaks due to the splitting of the Ru-d orbitals into sets of t_{2g}- and e_g-symmetry by the cubic crystal field.

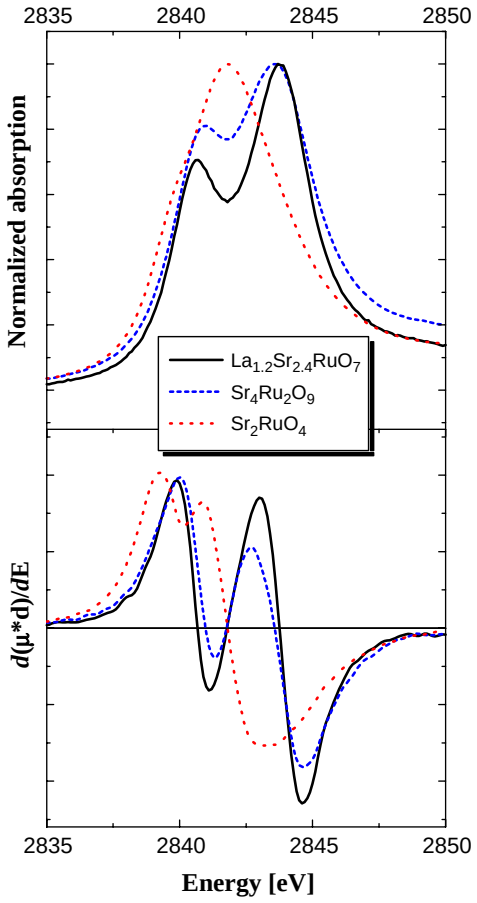

Fig. 7. Ru–L_{III} XANES of $La_{1.2}Sr_{2.4}RuO_7$ in comparison to selected Ru^{+4}- and Ru^{+5}-references. Upper and lower panels show the original spectra and their derivatives, respectively. For a better comparability the spectra have been normalized.

Fig. 7 shows the Ru−L_{III} XANES spectra and their first derivatives of $La_{1.2}Sr_{2.4}RuO_7$ in comparison to two selected reference samples containing Ru^{+4} and Ru^{+5} ions, respectively. As can be seen, the positions of the two white lines of $La_{1.2}Sr_{2.4}RuO_7$ are almost identical to the ones of the Ru^{+5} reference. A quantitative analysis according to the procedure given in Ref. [12] yielded energy positions of 2.8406 and 2.8438 keV for the t_{2g}- and e_g-related white lines, respectively. These values are very close to the results obtained for numerous Ru^{+5} reference compounds, including $Ba_5Ru_2O_9(O_2)$, $Sr_4Ru_2O_9$, and $La_{0.48}Sr_{1.52}Cu_{0.6}Ru_{0.4}O_{3.84}$ [8], for which values of 2.8404–2.8406 keV and 2.8435–2.8436 keV were found [12]. This very good agreement clearly indicates that the oxidation state of ruthenium actually is +5 in $La_{1.2}Sr_{2.4}RuO_7$.

4. Conclusions

Single crystalline $La_{1.2}Sr_{2.4}RuO_7$ was flux-grown and its structure was solved by X-ray diffraction. The compound is the first ruthenium containing $n = 2$ member of the $[A_2O][A_nB_{n-1}O_{3n}]$ family of hexagonal perovskites. Up to now, very few examples for this class of compounds are known. While $Ba_5Ru_2O_{10}$ is an $n = 3$ member of this series, the only $n = 2$ analogue known so far is $La_2Ca_2MnO_7$.

The structure of $La_{1.2}Sr_{2.4}RuO_7$ consists of layers of isolated RuO_6-octahedra separated by (Sr,La)O_6-prisms. These prisms form hexagonal vacancies, the centers of which are occupied by a single distorted oxygen ion. For the A-type cations in the trigonal prisms a split model was applied with parts of the Sr/La ions positioned on the *c*-axis and additional Sr ions occupying a distorted position close to this axis. Examinations of the valence shift in the Ru–L_{III} XANES spectra proved that the oxidation state of ruthenium is +5. This result was confirmed by magnetic measurements, which yielded a magnetic moment characteristic for Ru^{+5} ions. These measurements also revealed a medium-strength antiferromagnetic interaction of the magnetic moments. Since the Ru ions are isolated from each other and have quite long distances of 5.76 and 6.94 Å, respectively, this interaction is rather unusual, even though a similar magnetic behavior was already found for two structurally related ruthenates.

Acknowledgments

Thanks are due to HASYLAB for allocating beamtime and to Ms. B. Cornelisen for the EMA measurements. This work was supported by the Deutsche Forschungsgemeinschaft through SFB 484.

References

[1] J.M. Perez-Mato, M. Zakhour-Nakhl, J. Darriet, J. Mater. Chem. 9 (1999) 2795.
[2] K.E. Stitzer, J. Darriet, H.-C. zur Loye, Curr. Opin. Solid State Mater. Sci. 5 (2001) 535.
[3] F. Grasset, M. Zakhour, J. Darriet, J. Alloys Compd. 287 (1999) 25.
[4] C. Dussarrat, J. Fompeyrine, J. Darriet, Eur. J. Solid State Inorg. Chem. 31 (1994) 289.
[5] Y. Wang, J. Lin, Y. Du, R. Qin, B. Han, C.K. Loong, Angew. Chem. Int. Ed. 39 (2000) 2730.
[6] F. Grasset, C. Dussarrat, J. Darriet, J. Mater. Chem. 7 (1997) 1911.
[7] E. Gaudin, G. Goglio, A. Besnard, J. Darriet, J. Solid State Chem. 175 (2003) 124.
[8] S. Ebbinghaus, A. Reller, Solid State Ionics 101–103 (1997) 1369.
[9] J. de Meulenaer, H. Tompa, Acta Crystallogr. 19 (1965) 1014.
[10] G.M. Sheldrick, SHELXS97, Program for Crystal Structure Solution, University of Göttingen, 1997.
[11] G.M. Sheldrick, SHELXL97, Program for Crystal Structure Refinement, University of Göttingen, 1997.
[12] S. Ebbinghaus, Z. Hu, A. Reller, J. Solid State Chem. 156 (2001) 194.
[13] I.D. Brown, D. Altermatt, Acta Crystallogr. Sect. B 41 (1985) 244.
[14] C. Dussarrat, F. Grasset, R. Bontchev, J. Darriet, J. Alloys Compd. 233 (1996) 15.
[15] P. Khalifah, Q. Huang, D.M. Ho, H.W. Zandbergen, R.J. Cava, J. Solid State Chem. 155 (2000) 189.
[16] J.-H. Choy, J.-Y. Kim, S.-H. Hwang, S.-J. Kim, G. Demazeau, Int. J. Inorg. Mater. 2 (2000) 61.